Journal of Inorganic Biochemistry 195 (2019) 39–50

Contents lists available at ScienceDirect

Journal of Inorganic Biochemistry

journal homepage: www.elsevier.com/locate/jinorgbio

Structures and anticancer activity of chlorido platinum(II) saccharinate complexes with mono- and dialkylphenylphosphines

Ceyda Icsel[a], Veysel T. Yilmaz[a,*], Buse Cevatemre[b], Muhittin Aygun[c], Engin Ulukaya[d]

[a] Department of Chemistry, Faculty of Arts and Sciences, Uludag University, 16059 Bursa, Turkey
[b] Koc University Research Center for Translational Medicine (KUTTAM), 34450 Istanbul, Turkey
[c] Department of Physics, Faculty of Sciences, Dokuz Eylul University, 35210 Izmir, Turkey
[d] Department of Medicinal Biochemistry, Faculty of Medicine, University of Istinye, 34010 Istanbul, Turkey

ARTICLE INFO

Keywords:
Pt(II) complex
Saccharinate
Phosphine
DNA binding
Cytotoxicity
Anticancer mechanism

ABSTRACT

cis-[PtCl(sac)(PPh_2Me)$_2$] (**1**), *cis*-[PtCl(sac)($PPhMe_2$)$_2$] (**2**), *trans*-[PtCl(sac)(PPh_2Et)$_2$] (**3**) and *trans*-[PtCl(sac)($PPhEt_2$)$_2$] (**4**) complexes (sac = saccharinate) were synthesized and characterized by elemental analysis and spectroscopic methods. The structures of **2–4** were determined by X-ray single-crystal diffraction. The interaction of the complexes with DNA was studied various biochemical, biophysical and molecular docking methods. Only the *cis*-configured complexes (**1** and **2**) showed nuclease activity and their binding affinity towards DNA was considerably higher than those of their *trans*-congeners (**3** and **4**). The chlorido ligand in the *cis*-configured complexes underwent aquation, making them more reactive towards DNA. Furthermore, **1** and **2** exhibited anticancer potency on breast (MCF-7) and colon (HCT116) cancer cells similar to cisplatin, whereas **3** and **4** were biologicallly inactive. Mechanistic studies on MCF-7 cells showed that higher nuclear uptake, cell cycle arrest at the S phase, dramatically increased DNA double-strand breaks, apoptosis induction, elevated levels of reactive oxygen species (ROS) and high mitochondrial membrane depolarization greatly contribute to the anticancer potency of **1** and **2**.

1. Introduction

Platinum-based coordination compounds became important chemotherapeutic drugs in cancer therapy. Investigations in this field were dominated by the use of cisplatin in clinical treatments. It is well-established that the chemical reactivity and anticancer properties of the platinum complexes can vary significantly with their stereochemistry. For instance, cisplatin is highly cytotoxic at the relatively low doses, whereas its *trans* isomer is practically inactive [1]. However, dose-limiting toxic side effects and drug resistance are the main limitations of cisplatin in chemotherapy [2]. Then, the later-generation cisplatin analogues, carboplatin and oxaliplatin, were clinically introduced with reduced toxic side effects and improved chemotherapeutic efficacy. The clinically used Pt drugs have two *cis* oriented inert ammine or chelating diamine ligands together with two relatively labile chlorido ligands or oxygen donor chelating ligands. They exert their cytotoxic activity via covalent binding to DNA after losing the two leaving ligands.

Metal complexes of the artificial sweetener saccharin (sacH, o-sulphobenzimide), in particular those of palladium(II) and platinum(II), are of interest to us as potent anticancer agents. We reported a number of Pd(II) and Pt(II) sac complexes derived from pyridine-based ligands, showing considerable anticancer activity [3–5]. Mechanistic studies demonstrated that these complexes induce apoptosis in cancer cells and tumors [6–10]. Furthermore, the anticancer potentials of Pd(II) and Pt(II) complexes of sac also received much attention from other research groups [11–13]. On the other hand, Pt(II) complexes of phosphines were evaluated as potential anticancer agents [14–17], although some of them were biologically inactive [14,18,19]. The Pt(II) complexes of sac containing phosphine ligands are rare and only two papers on the synthesis and structures of Pt(II) sac complexes of mono- and diphosphines appeared in the literature [20,21].

As part of our continuing research, we designed and synthesized novel Pd(II) and Pt(II) sac complexes bearing mono- and diphoshine ligands. Some of these complexes with tertiary phosphines containing phenyl (Ph)/cyclohexyl (Cy) groups [22] and bis(diphenylphosphino) alkanes [23,24] showed promising cytotoxicity and cause apoptotic cell death due to over generation of reactive oxygen species (ROS), damaging to mitochondria and DNA. In the present paper, we expand the work to the synthesis of new chlorido platinum(II) sac complexes with monophosphines PPh_2R and $PPhR_2$, where R is Me or Et (Scheme 1).

* Corresponding author.
E-mail address: vtyilmaz@uludag.edu.tr (V.T. Yilmaz).

https://doi.org/10.1016/j.jinorgbio.2019.03.008
Received 29 January 2019; Received in revised form 7 March 2019; Accepted 8 March 2019
Available online 14 March 2019

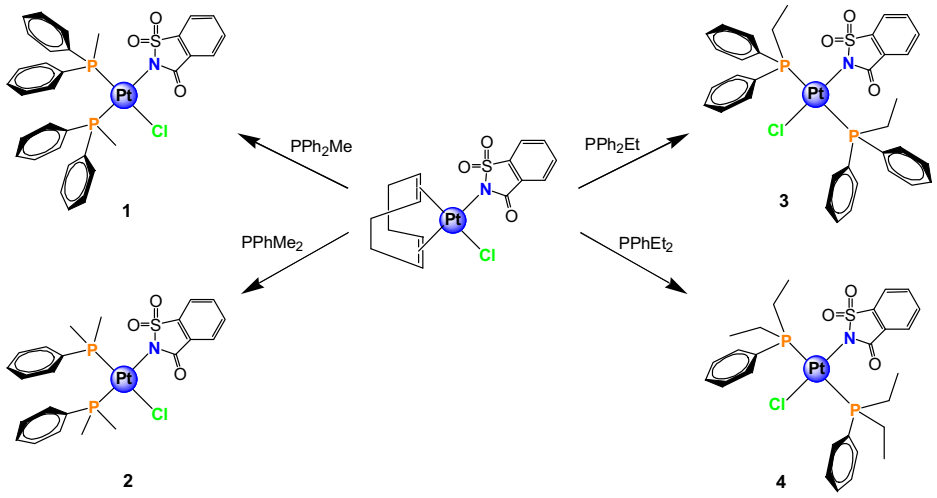

Scheme 1. Synthesis and structures of the platinum(II) sac complexes with PPh_2R and $PPhR_2$ (R = Me or Et).

The Pt(II) complexes of the phosphines containing the Me group display the *cis* configuration, while those of with the Et group are *trans* isomers. The *cis*-configured complexes exhibited significant anticancer activity, whereas their *trans*-configured counterparts were inactive. The effect of the phosphine ligands on the stereochemistry and biological activity of the complexes was discussed. The interaction of the complexes with DNA was studied using various biochemical and biophysical techniques. The lipophilicity and cellular uptake of the complexes were explored. In addition, the anticancer mechanism of the potent complexes was investigated in detail using Hoechst 33342 staining and flow cytometry.

2. Experimental

2.1. Materials and measurements

All reagents were purchased commercially and used as received. Elemental analyses for C, H, and N were performed using a Costech elemental analyzer. UV–vis and IR spectra were obtained using a Perkin Elmer Lambda 35 and a Perkin Elmer Spectrum Two FT-IR spectrophotometers, respectively. ^{1}H, ^{13}C and ^{31}P NMR spectra were recorded on a Bruker Avance III (400.13 MHz ^{1}H; 100.62 MHz ^{13}C and 161.97 MHz ^{31}P) NMR spectrometer in DMSO-d_6 at room temperature (rt). Fluorescence spectra were recorded with a Varian Cary Eclipse spectrophotometer equipped with a Xe pulse lamp of 75 kW. The excitation and emission slits were 5 nm. The ESI mass spectra were recorded using a Bruker Daltonics Microtof II-ESI-TOF mass spectrometer. The electrical conductivity measurements of the complexes in MeOH were carried out with HANNA HI 5521 at rt. Melting points are measured using a BUCHI 560 instrument.

2.2. Synthesis of platinum complexes

The phosphine ligand (PPh_2R and $PPhR_2$; R = Me or Et) (0.5 mmol) was directly added to the solution of the starting complex [PtCl(sac)(COD)] (COD = 1,5-cyclooctadiene) (0.25 mmol, 0.13 g) in the mixture of MeCN and MeOH (1:1, 10 mL). The reaction mixture was refluxed for 24 h. Then, the solvents were removed by a rotary evaporator and the white solids were washed with diethyl ether and a small amount of cold EtOH. The solids were dissolved in a mixture containing water, MeCN and MeOH (1:1:1). The crystals of **2**, **3** and **4** were obtained from the evaporation of the solutions after three or four weeks at r.t.

cis-[PtCl(sac)(PPh_2Me)$_2$] (**1**). Yield: 118 mg (58%). Mp 172–176 °C. Anal. calc. for $C_{33}H_{30}ClNO_3P_2PtS$ (%): C, 48.74; H, 3.72; N, 1.72. Found C, 48.61; H, 3.57; N, 1.89. IR (ν/cm^{-1}): 3058w, 2920w, 2878vw, 2826vw, 1669 m (CO), 1591w, 1482w, 1459w, 1436 m (CC), 1330w ν_s(CNS), 1287s, 1246 m $\nu_{as}(SO_2)$, 1171s, 1154s $\nu_s(SO_2)$, 1122 m, 1103s, 1058w, 1058w, 1029w, 999w (PC_{sym}), 964 m ν_{as}(CNS), 892 s, 792 m, 736 s (γCH), 693 s, 678 s γ(ring-Ph), 596vs, 561 m, 539 m, 520vs, 506vs (PC_{asym}), 490 s, 455 s, 433 m, 417 m. ^{1}H NMR (400.13 MHz, DMSO-d_6, δ, ppm): 7.97–7.15 (m, 20H, Ph protons of PPh_2Me and 4H, sac), 2.06–1.75 (m, 6H, CH_3-PPh_2Me). ^{13}C NMR (100.62 MHz, DMSO-d_6, δ, ppm): 164.9 (C_7-sac), 142.5 (C_1-sac), 133.6 (s, C_{ipso}-Ph), 133.0 (C_3-sac), 132.6 (d, C_{ortho}-Ph, J_{PC} = 11 Hz), 131.3 (s, C_{para}-Ph), 130.7 (C_6-sac), 129.0 (m, C_{metha}-Ph and C_4-sac), 123.7 (C_5-sac), 120.1 (C_2-sac), 15.3(s, CH_3-P_aPh_2Me), 14.0 (s, CH_3-P_bPh_2Me). ^{31}P NMR (161.97 MHz, DMSO-d_6, δ, ppm): 0.28 (d, $^{1}J_{PtPa}$ = 3411.7 Hz, $^{2}J_{PaPb}$ = 19.4 Hz), −6.75 (d, $^{1}J_{PtPb}$ = 3666.1 Hz, $^{2}J_{PbPa}$ = 19.4 Hz). UV–vis (MeOH) λ_{max}/nm (ε_{max}/M^{-1} cm^{-1}) 266 (21830), 274 (18819). Molar conductivity, Λ_M (MeOH, 298 K, 10^{-3} M) 5 S cm^2 mol^{-1} (nonelectrolyte). ESI–MS (*m/z*, MeOH): 777.9 (65%, calc. 777.7) [M − Cl]$^+$, 705.7 (21%, calc. 705.6) [Pt(sac)(PPh_2Me)(MeOH)$_4$]$^+$, 673.4 (59%, calc. 673.6) [Pt(sac)(PPh_2Me)(MeOH)$_3$]$^+$, 630.8 (94%, calc. 631.0) [M − sac]$^+$, 505.3 (100%, calc. 505.4) [Pt(sac)(MeOH)$_4$]$^+$.

cis-[PtCl(sac)($PPhMe_2$)$_2$] (**2**). Yield: 86 mg (50%). Mp 189–192 °C (decomp.). Anal. calc. for $C_{23}H_{26}ClNO_3P_2PtS$ (%): C, 40.09; H, 3.80; N, 2.03. Found C, 40.32; H, 3.98; N, 2.21. IR (ν/cm^{-1}): 3091vw, 3008vw, 2916w, 1675s (CO), 1589 m, 1483w, 1459w, 1439 m, 1420 m (CC), 1325w ν_s(CNS), 1305s, 1283vs, 1240s $\nu_{as}(SO_2)$, 1172s, 1152vs, 1143vs $\nu_s(SO_2)$, 1109s, 1057 m, 999w (PC_{sym}), 966 s, 951 s ν_{as}(CNS), 910vs, 849 m, 789 s, 757vs (γCH), 716 s, 702 s, 678 s γ(ring-Ph), 657 m, 597vs, 558 s, 540 s, 520 s (PC_{asym}), 489vs, 453 s, 439 m, 417 m. ^{1}H NMR (400.13 MHz, DMSO-d_6, δ, ppm): 8.05–7.33 (m, 10H, Ph protons of $PPhMe_2$ and 4H, sac), 1.92–1.31 (m, 12H, CH_3-$PPhMe_2$). ^{13}C NMR (100.62 MHz, DMSO-d_6, δ, ppm): 164.9 (C_7-sac), 142.4 (C_1-sac), 133.9 (s, C_{ipso}-Ph), 132.1 (C_3-sac), 132.0 (C_6-sac), 131.8 (d, C_{ortho}-Ph, J_{PC} = 11 Hz), 131.4 (s, C_{para}-Ph), 129.2 (C_4-sac), 128.8 (d, C_{metha}-Ph, J_{PC} = 11 Hz), 123.8 (C_5-sac), 120.7 (C_2-sac), 14.3 (s, CH_3-P_aPhMe_2), 13.2 (s, CH_3-P_bPhMe_2). ^{31}P NMR (161.97 MHz, DMSO-d_6, δ, ppm): −10.8 (d, $^{1}J_{PtPa}$ = 3367.9 Hz, $^{2}J_{PaPb}$ = 21.1 Hz), −18.0 (d, $^{1}J_{PtPb}$ = 3594.8 Hz, $^{2}J_{PbPa}$ = 21.1 Hz). UV–vis (MeOH) λ_{max}/nm (ε_{max}/M^{-1} cm^{-1}) 266 (15140), 272 (13896). Molar conductivity, Λ_M (MeOH, 298 K, 10^{-3} M) 4 S cm^2 mol^{-1} (nonelectrolyte). ESI–MS (*m/z*, MeOH): 1342.8 (7%, calc. 1342.6) [2 M − Cl]$^+$, 1195.2 (8%, calc. 1195.1) [2 M − sac]$^+$, 711.9 (4%, calc. 712.0) [M + Na]$^+$, 653.7 (100%, calc. 653.6) [M − Cl]$^+$, 579.6 (34%, calc. 579.5) [Pt(sac)($PPhMe_2$)(MeOH)$_2$]$^+$, 547.5 (41%, calc. 547.4) [Pt(sac)($PPhMe_2$)(MeOH)]$^+$, 506.6 (64%, calc. 506.8) [M − sac]$^+$, 441.7 (55%, calc. 441.3) [Pt(sac)(MeOH)$_2$]$^+$.

trans-[PtCl(sac)(PPh_2Et)$_2$] (**3**). Yield: 133 mg (63%). Mp 237–240 °C. Anal. calc. for $C_{35}H_{34}ClNO_3P_2PtS$ (%): C, 49.97; H, 4.07; N,

1.67. Found C, 50.18; H, 4.15; N, 1.86. IR (ν/cm^{-1}): 3064w, 2973vw, 2930vw, 2877vw, 1673s (CO), 1595w, 1484w, 1458w, 1433 m (CC), 1334w ν_s(CNS), 1297vs, 1257 m ν_{as}(SO_2), 1173 m, 1153vs ν_s(SO_2), 1120 m, 1103s, 1057w, 1034 m, 1011w, 999 m (PC_{sym}), 968 s ν_{as}(CNS), 803w, 793w, 764 m, 748vs, 737 s (γCH), 712 s, 691vs, 679vs γ(ring-Ph), 659 m, 595vs, 564 s, 535 s, 513vs (PC_{asym}), 484 s, 466 s, 449 s, 437 s, 425 m, 413 m, 403w. ^{1}H NMR (400.13 MHz, DMSO-d_6, δ, ppm): 7.87–7.13 (m, 20H, Ph protons of PPh_2Et and 4H, sac), 2.61–2.25 (m, 4H, CH_2-PPh_2Et), 1.29–0.81 (m, 6H, CH_3-PPh_2Et). ^{13}C NMR (100.62 MHz, DMSO-d_6, δ, ppm): 164.8 (C_7-sac), 140.8 (C_1-sac), 134.2 (t, C_{ipso}-Ph, J_{PC} = 6 and 6 Hz), 133.6 (t, C_{ortho}-Ph, J_{PC} = 6 and 6 Hz), 133.2 (C_3-sac), 131.0 (C_6-sac), 130.9 (s, C_{para}-Ph), 129.5 (C_4-sac), 128.5 (td, C_{metha}-Ph, J_{PC} = 5 and 5 Hz), 123.5 (C_5-sac), 120.4 (C_2-sac), 17.9 (d, CH_2-PPh_2Et, J_{PC} = 19 Hz), 8.9 (s, CH_3-PPh_2Et). ^{31}P NMR (161.97 MHz, DMSO-d_6, δ, ppm): 15.8 (s, $^1J_{PtP}$ = 2514.2 Hz). UV–vis (MeOH) λ_{max}/nm (ε_{max}/M^{-1} cm^{-1}) 269 (32294). Molar conductivity, Λ_M (MeOH, 298 K, 10^{-3} M) 4 S cm^2 mol^{-1} (nonelectrolyte). ESI–MS (*m/z*, MeOH): 874.2 (100%, calc. 874.1) [M(MeOH) + H]$^+$, 842.1 (10%, calc. 842.2) [M + H]$^+$, 659.3 (17%, calc. 659.0) [M – sac]$^+$.

trans-[PtCl(sac)($PPhEt_2$)$_2$] (**4**). Yield: 140 mg (75%). Mp 171–175 °C. Anal. calc. for $C_{27}H_{34}ClNO_3P_2PtS$ (%): C, 43.52; H, 4.60; N, 1.88. Found C, 43.35; H, 4.52; N, 2.03. IR (ν/cm^{-1}): 3068vw, 2967w, 2936w, 2879w, 1683s (CO), 1593w, 1483w, 1456 m, 1437 m (CC), 1337w ν_s(CNS), 1300s, 1287s, 1248s ν_{as}(SO_2), 1172s, 1151vs ν_s(SO_2), 1123 m, 1112 m, 1030s, 1005w (PC_{sym}), 968 s ν_{as}(CNS), 800w, 793w, 771 m, 755 s, 735 s (γCH), 717vs, 691 s, 677 s γ(ring-Ph), 642 m, 597vs, 563vs, 536 s, 518 s (PC_{asym}), 494vs, 474 s, 463 m, 449w, 422w, 409w. ^{1}H NMR (400.13 MHz, DMSO-d_6, δ, ppm): 8.08–7.28 (m, 10H, Ph protons of $PPhEt_2$ and 4H, sac), 2.38–1.80 (m, 8H, CH_2-$PPhEt_2$), 1.21–0.52 (m, 12H, CH_3-$PPhEt_2$). ^{13}C NMR (100.62 MHz, DMSO-d_6, δ, ppm): 164.8 (C_7-sac), 140.9 (C_1-sac), 134.2 (s, C_{ipso}-Ph), 133.9 (C_3-sac), 132.9 (t, C_{ortho}-Ph, J_{PC} = 6 and 6 Hz), 130.7 (C_6-sac), 130.2 (s, C_{para}-Ph), 129.4 (C_4-sac), 128.6 (t, C_{metha}-Ph, J_{PC} = 6 and 6 Hz), 124.1 (C_5-sac), 120.9 (C_2-sac), 13.4 (dt, CH_2– $PPhEt_2$, J_{PC} = 17 and 17 Hz), 7.7 (d, CH_3-$PPhEt_2$, J_{PC} = 8 Hz). ^{31}P NMR (161.97 MHz, DMSO-d_6, δ, ppm): 14.9 (s, $^1J_{PtP}$ = 2428.4 Hz). UV–vis (MeOH) λ_{max}/nm (ε_{max}/M^{-1} cm^{-1}) 262 (27434). Molar conductivity, Λ_M (MeOH, 298 K, 10^{-3} M) 4 S cm^2 mol^{-1} (nonelectrolyte). ESI–MS (*m/z*, MeOH): 768.0 (12%, calc. 768.1) [M + Na]$^+$, 746.0 (32%, calc. 746.1) [M + H]$^+$, 709.9 (80%, calc. 709.7) [M – Cl]$^+$, 606.7 (37%, calc. 607.1) [Pt(sac)($PPhEt_2$)(MeOH)$_2$]$^+$, 574.9 (39%, calc. 575.5) [Pt(sac)($PPhEt_2$)(MeOH)]$^+$, 562.7 (100%, calc. 562.9) [M – sac]$^+$, 558.3 (17%, calc. 558.5) [Pt($PPhEt_2$)$_2$(MeOH) -H]$^+$.

2.3. Hydrolysis studies

UV–vis spectra of the solutions of **2** and **4** with final concentrations of 20 μM in MeOH/H_2O (1/1, v/v) were recorded at 298 K at various time intervals. Moreover, complexes **2** and **4** were dissolved in DMSO-d_6 and then mixed with D_2O to give a final concentration of 1 mM in 70% DMSO-d_6/30% D_2O (v/v). ^{1}H NMR spectra were recorded after various time intervals at r.t. At 24 h, an excess of NaCl (100 mM) was added to the solution of the complexes and then, ^{1}H NMR spectra were recorded.

2.4. X-ray diffraction

The data collection was performed on a Rigaku Xcalibur X-ray diffractometer with EOS CCD detector using Mo-K_α radiation (0.71073 Å) with ω-scan mode. The structures were solved with the ShelXT structure solution program [25], and refined by a full-matrix least-squares minimization with the ShelXL refinement package [26], using Olex2 [27]. All non-hydrogen atoms were refined anisotropically, while all hydrogen atoms were located at calculated positions and refined by using riding model. Details of the data collection and structure refinement are given in Table S1.

Crystallographic data and refinement parameters of the reported structures (**2**, **3** and **4**) have been deposited at the Cambridge Crystallographic Data Centre with CCDC numbers 1869332–1869334. These data can be obtained free of charge via www.ccdc.cam.ac.uk/data_request/cif, or by emailing data_request@ccdc.cam.ac.uk, or by contacting The Cambridge Crystallographic Data Centre, 12 Union Road, Cambridge CB2 1EZ, UK; fax: +44 1223 336033.

2.5. Partition coefficients

Partition coefficients of **1**–**4** and cisplatin in n-octanol/water were determined by the classical shake flask method using the standard protocol [28]. Two parallel experiments were performed for each sample and the amount of the complexes in the n-octanol phase was analyzed by UV–vis measurements. Partition coefficient (log *P*) defined as the logarithmic ratio of the equilibrium concentrations of the dissolved complex between the organic and aqueous phases (log C_O/C_W) was estimated.

2.6. Cellular uptake

MCF-7 cells were selected for uptake studies. The cells were exposed to 25 μM of **1**–**4** and cisplatin at 37 °C for 4 h. Then, the incubation medium was removed and the cells were washed with cold phosphate-buffered saline twice, tyripsinized and the cell suspension was counted. The FractionPREP kit (BioVision) was used to isolate subcellular fractions (cytosol, nucleus, membrane/particulate and cytoskeletal) according to the supplier's instructions. 2.5 mL of ultrapure HNO_3 (69%) were added to the fractions and the solutions were heated to dryness. Then, the solids were dissolved in 1 mL of HCl (37%) and heated to dryness to remove traces of HNO_3. The Pt content in each fraction was determined by the differential pulse stripping voltammetry, according to the method reported in the literature [29], using an Epsilon electrochemical workstation with a conventional three electrode system with hanging mercury drop working electrode, a glassy carbon auxiliary electrode and a Ag/AgCl reference electrode. Each measurement was repeated three times and the results were expressed as pmol Pt complex/10^6 cells.

2.7. DNA binding studies

The stock solution of fish sperm (FS) DNA was prepared in Tris-HCl buffer (20 mM Tris-HCl/NaCl, pH = 7.0), while complexes **1**–**4** were dissolved in MeOH. UV absorption titration experiments were performed by varying the concentration of the complexes in the range of 0–25 μM and maintaining the concentration of FS-DNA at 50 μM. The intrinsic binding constants (K_b) were calculated using the Benesi-Hildebrand equation [30].

$$1/(A–A_0) = 1/\{K_b(A_{max}–A_0)[Q]\} + 1/[A_{max}–A_0]$$

where A_0 is the absorption intensity of DNA, A is the absorption intensity of DNA interacted with a metal complex, A_{max} is the saturated absorption intensity of the DNA–metal complex adduct and [Q] is the concentration of the metal complex. The binding constant (K_b) was graphically evaluated by plotting 1/[A–A_0] versus 1/[Q].

In fluorescence titration experiments, **1**–**4** (0–50 μM) were added to FS-DNA solutions pre-treated with ethidium bromide (EB) (NP/EB = 10) in Tris-HCl. The emission spectra of these solutions were recorded upon excitation at λ_{ex} = 295 nm, and 293, 297 and 300 K. The quenching constants (K_{SV}) were determined using the Stern-Volmer equation [31].

$$F_0/F = 1 + K_{SV}[Q]$$

where F_0 and F are the fluorescence intensities in the absence and presence of the complexes, respectively. [Q] is the total concentration of the quencher (metal complex).

The apparent binding constant (K_{app}) was estimated from the following equation [32].

$$K_{EB}[EB] = K_{app}[Q]$$

in which [Q] is the concentration of the quencher causing a 50% reduction in the fluorescence intensity of EB-bound DNA, $K_{EB} = 1.0 \times 10^7\ M^{-1}$.

The binding constant K_F is determined from the Scatchard equation [33].

$$\log(F_0 - F)/F = \log K_F + n \log[Q]$$

The plot of $\log(F_0\text{-}F)/F$ versus log[Q] is drawn and fitted linearly and the number of binding site (n) per nucleotide was obtained from the slope.

The relative viscosity of FS-DNA solutions (0.8 mM bp) with increasing amounts of **1–4** was measured using an Ubbelohde viscometer at 20 °C. Viscosity values were calculated from the observed flow time of DNA-containing solutions (t) corrected for the flow time of buffer alone (t_0), $\eta = t - t_0$.

2.8. Gel electrophoresis assay

The nuclease activity of **1–4** was performed agarose gel electrophoresis after incubation of the samples containing 100 ng plasmid DNA in 50 mM Tris-HCl/NaCl buffer (pH 7.2) with the complexes (0, 25, 50 and 100 μM) at 37 °C for 4 h. To clarify the DNA groove binding preferences of the complexes, the plasmid DNA was incubated with DAPI (4′,6-diamidino-2-phenylindole) and MG (methyl green) (100 μM) for 1 h and then to the solution, **1–4** (100 μM) were added. The final solutions were incubated another 3 h. In restriction enzyme inhibition studies, the plasmid DNA was incubated with 50 μM of the complexes at 37 °C in the buffer (pH 7.2) for 1 h. The resulting solutions were subsequently incubated separately with *Hin*dIII and *Bam*HI (2 units) for 15 min. The samples were electrophoresed for 45 min at 120 V on 1.0% agarose gel using 1 × TBE (Tris-borate-EDTA) buffer (pH 8.0). The gels were then stained using 1 μg/mL EB and photographed under UV light.

2.9. Molecular docking

Molecular docking studies were carried out using Autodock/Vina [34]. The crystal structure of 1BNA $(CGCGAATTCGCG)_2$ was taken from the Protein Data Bank. The binding site was centred on the DNA and a grid box was created with 60 × 60 × 60 points and a 0.375 Å grid spacing in which almost the entire macromolecules were involved. For each docking calculation, 10 different poses were required within the energy range of 2 kcal mol^{-1}. All other parameters were kept at their default values. The docked molecules were visualized by Discovery Studio 3.5 software.

2.10. Biological evaluation assays

2.10.1. Cell culture

The human breast cancer (MCF-7), lung cancer (A549), colon cancer (HCT116) and normal bronchial epithelial cells (BEAS-2B) were purchased from American Type Culture Collection (ATCC) and cultured with RPMI 1640 culture media supplemented with penicillin G (100 U/mL), streptomycin (100 μg/mL), L-glutamine, and 10% fetal bovine serum at 37 °C in a humidified atmosphere containing 5% CO_2. The stock solutions of **1–4** (40 mM) were prepared in DMSO, while the clinically-used formulation of cisplatin (0.5 mg/mL of saline) was used as a stock solution. Further dilutions were made in cell culture medium. In order to avoid the toxic effect of DMSO on cells, the final concentration of DMSO was kept at < 0.1%.

2.10.2. SRB and ATP viability tests

In the Sulforhodamine B (SRB) assay, cells were seeded in 96 well plate at the density of 5×10^3 cells/well and exposed to 20 μM dose of the complexes for 48 h. Then, cells were in situ fixed with 50 μL of 50% (w/v) trichloroacetic acid at 4 °C for 1 h. Wells were washed 5 times with deionized water and allowed air dry at rt. 50 μL of 0.4% SRB solution were added into each well and incubated at rt. for 30 min. Then, plates were washed with 1% acetic acid to eliminate non-specific bindings and unbounded dye. The bounded SRB dye was dissolved by adding 150 μL 10 mM Tris base per each well. Measurements were carried out at 564 nm using Lumistar Omega microplate reader. Experiments were performed in triplicate.

In order to determine cell viability using the ATP assay, the cells were seeded 5×10^3 cells /well and treated for 48 h. with the potent complexes (**1–4**), which were found to be effective according to the SRB cytotoxicity test. The ATP content in the treated cells and control cells was measured using a luminometer (Lumistar Omega microplate reader) with a measuring time of 1 s. The results were obtained as relative light unit (RLU) and viability was calculated by the following formula:

$$\text{Viability (\%)} = [100 \times (\text{Sample RLU})/(\text{Control RLU})]$$

2.10.3. Nuclear staining assay

MCF-7 cells (5×10^3 cells/well) were exposed to the IC_{90} doses of **1** (27.2 μM), **2** (44.5 μM) and cisplatin (28.0 μM) for 12 and 24 h. The cells were then stained with 10 μM Hoechst 33342 and examined under fluorescence microscope.

2.10.4. Flow cytometric assays

MCF-7 cells were plated at 3×10^5 cells per well (in duplicate) into 6-well plates and treated with the IC_{90} doses of **1**, **2** and cisplatin for 24 and 48 h. Cell cycle distribution, generation of ROS, cellular apoptosis, mitochondrial membrane depolarization and DNA damage (Phosphorylation of histone H2AX) were determined by a Muse Cell Analyzer, using Muse Cell Cycle Assay Kit (MCH100106, Millipore), Muse Oxidative Stress Kit (MCH100111-2, Millipore), Muse Annexin V and Dead Cell Kit (MCH100105, Millipore), and caspase 3/7 kit (MCH100108, Millipore) Muse Mito Potential Assay Kit (MCH100110, Millipore) and Muse H2AX Activation Dual Detection Kit (MCH200101, Millipore), respectively, according to the manufacturer's instructions.

3. Results and discussion

3.1. Synthesis and spectroscopy

The reaction between Na(sac) in MeOH, and $[PtCl_2(COD)]$ in CH_2Cl_2 leads to the starting complex [PtCl(sac)(COD)]. The reactions of PPh_2Me, $PPhMe_2$ PPh_2Et and $PPhEt_2$ with the platinum precursor are based on the ligand exchange between COD and the phosphines, giving *cis*-$[PtCl(sac)(PPh_2Me)_2]$ (**1**), *cis*-$[PtCl(sac)(PPhMe_2)_2]$ (**2**), *trans*-$[PtCl(sac)(PPh_2Et)_2]$ (**3**) and *trans*-$[PtCl(sac)(PPhEt_2)_2]$ (**4**) in moderate- to-good yields (Scheme 1). The *cis/trans* isomerisation in **1–4** may be explained by the reaction of the starting complex with MeCN used as a solvent in the synthesis of the complexes. The chlorido Pt(II) complexes of MeCN was obtained in both *cis* and *trans* forms [35]. Compared to those of PPh_2Me and $PPhMe_2$, the higher basicity of PPh_2Et and $PPhEt_2$ results in the thermodynamically more stable *trans*-configured complexes of **3** and **4** [35,36]. Furthermore, the relatively higher cone angles of PPh_2Et and $PPhEt_2$ may also favour the *trans* configuration to reduce the steric hindrance [37]. Overall, one or all of these reasons may be responsible for the different geometrical isomerism in **1–4**. The complexes were crystallized from a mixture of water, MeCN and MeOH (1:1:1). All the attempts to obtain crystals of **1** failed. The complexes are air-stable and soluble in MeCN, MeOH, DMSO and DMF as well as in the aqueous solutions of these solvents. Electrical conductivity measurements in MeOH indicate the non-electrolyte behaviour of **1–4**.

Several spectroscopic techniques were used to confirm the

formation of the platinum complexes. The ESI-MS$^+$ spectra of **1–4** show signals corresponding to the $[M - Cl]^+$, $[M - sac]^+$, $[M + H]^+$ and $[M + Na]^+$ species in solution (Fig. S1). The IR spectra display the characteristic strong bands of the carbonyl group of sac at ca. 1675 cm^{-1}. The $\nu_{as}(SO_2)$ and $\nu_s(SO_2)$ modes appear at ca. 1250 and 1150 cm^{-1}, respectively. The CH vibrations of the Ph, Me and Et groups of the phosphines occur in the range of 3090–2830 cm^{-1}, while ν_s(PC) and ν_{as}(PC) stretching absorptions are observed at ca. 1000 and 515 cm^{-1}, respectively (Fig. S2).

The stability and configurations of the platinum complexes in solution were studied by multinuclear NMR techniques (^{1}H, ^{13}C and ^{31}P) at rt. The NMR spectra of **1–4** confirm that in each case, only one isomer is present in solution (Fig. S3). Moreover, time-dependent ^{31}P NMR spectra measurements at 0, 24 and 48 h showed that all the complexes are highly stable in DMSO and no interconversion of the *trans* form to the *cis* form or vice versa is observed (Fig. S4). In addition, the time-dependent ^{1}H NMR measurements indicated that the complexes undergo no substitution of the chloride ligands by DMSO (Fig. S5).

In the ^{1}H NMR spectra, the signals of the aromatic protons of both sac and phosphines appear as multiplets in the range of 8.08–7.13 ppm. The protons of the Me group are observed as multiplets between 2.06 and 1.31 ppm, while two sets of well-resolved resonances in the range of 2.61–1.80 and 1.29–0.52 ppm are assigned to the CH_2 and CH_3 protons of the Et group. Both Me and Et protons experience notable deshielding due to coordination to Pt(II). In the ^{13}C NMR spectra, the C═O and C─S groups resonance at ca. 165 and 141 ppm, respectively. The signals in the range 134–120 ppm correspond to the phenyl C atoms. In addition, two resonances around 15.3 and 14.0 ppm for **1** and 14.3 and 13.2 ppm for **2** are assigned to the Me groups, indicating the *cis* configuration of PPh_2Me and $PPhMe_2$ around Pt(II). These observations are consistent with previous reports [38]. On the other hand, in the spectra of **3** and **4**, the CH_2 and CH_3 groups are well-resolved. The lower field resonances correspond to the CH_2 group, while the higher field signals are related to CH_3.

The ^{31}P{^{1}H} spectra of the ligands and complexes displayed well-defined signals. The signals of PPh_2Me, $PPhMe_2$, PPh_2Et and $PPhEt_2$ appear as a singlet at −28.0, −46.2, −13.3 and −16.8 ppm, respectively, and shift by approximately 24 to 31 ppm to the downfield upon coordination to Pt(II). The spectra of **1** and **2** present two doublets due to non-equivalent P nuclei in the *cis* position, while one P nucleus is observed in the case of **3** and **4**, confirming the *trans* configuration of the phosphine ligands (Figs. 1 and S3). In **1** and **2**, the two P atoms are *trans* to the chlorido ligand (P_a), and the N atom of sac (P_b). In the spectra of **1** and **2**, P_b is more shielded than P_a and the coupling of the P nuclei with the ^{195}Pt isotope gives a pair of characteristic satellite lines with an intensity of ca. 1:4:1. The $^1J_{PtP}$ coupling values associated with P_a/P_b are 3412/3666 Hz and 3368/3595 Hz for **1** and **2**, respectively, indicating that the *trans* influence of the Cl ligand is higher than that of sac. The $^2J_{PP}$ coupling values are estimated as 19.4 Hz for **1**, and 21.1 Hz for **2**. On the other hand, the P atoms in **3** and **4** appear as a singlet coupled to Pt to give two satellites with $^1J_{PtP}$ coupling values of 2514 and 2428 Hz, respectively. The magnitude of the $^1J_{PtP}$ constants corresponds well with the coupling data reported for the *cis* and *trans* isomers of chlorido platinum complexes bearing monophosphines [22,39–41].

3.2. Hydrolysis

The Pt—Cl bonds are susceptible to the ligand exchange reactions. In biological systems, aquation or hydrolysis of platinum complexes via the Pt—Cl bonds is an important step in the mechanism responsible for the anticancer activity of cisplatin, generating the more reactive aqua species $[PtCl(NH_3)_2(H_2O)]^+$ and $[Pt(NH_3)_2(H_2O)_2]^{2+}$ towards DNA [42]. Therefore, a *cis*- configured complex (**2**) and a *trans*-configured complex (**4**) were selected and their hydrolysis in MeOH/H_2O (1/1, v/v) was monitored by UV–Vis spectroscopy at 298 K. Time-dependent studies showed that the absorption bands of **2** decrease with time, while no absorbance changes are observed in the spectra of **4**, indicating only the hydrolysis of **2** (Fig. 2). Formation of the aqua adducts of **2** is fitted to pseudo first-order kinetics [43]. The hydrolysis rate constant (k) is 5.4×10^{-3} min^{-1} and the half-life of hydrolysis ($t_{1/2}$) is 128.4 min.

The hydrolysis of a *cis*- (**2**) and a *trans*-configured complex (**4**) dissolved in DMSO-d_6/D_2O (7/3, v/v) was further monitored by ^{1}H NMR spectroscopy at different time intervals up to 24 h at rt. The spectra of the complexes in DMSO-d_6 and DMSO-d_6/D_2O were compared to justify the hydrolysis of these complexes. As shown in Fig. S6, a singlet at 3.33 ppm is assigned to H_2O in DMSO-d_6 and this signal is shifted to 4.28 ppm in DMSO-d_6/D_2O. In the spectra of **2**, new signals with lower intensity appear around the main signal of H_2O and their intensity increases with time. The spectral changes in the aromatic region are also observed in agreement with the previous data [44,45]. These new signals are attributed to the formation of the aqua species of **2**, and disappear after the addition of NaCl (100 mM) to the solution of **2** at 24 h, suggesting the reversibility of the hydrolysis of **2** at high Cl^- concentrations. Contrary to those of **2**, the ^{1}H NMR spectra of **4** do not show any alterations over 24 h. These findings clearly indicate the hydrolysis of the *cis*-configured complexes, while the *trans*-configured complexes seem to be unreactive towards ligand substitution.

3.3. Crystallography

The structures of the complexes were further confirmed by X-ray crystallography. The single crystals of **2–4** were grown by slow evaporation of the saturated solutions of the complexes at rt. Complex **2** crystalizes in the monoclinic $P2_1/n$ space group, while **3** and **4** are isostructural and crystallize in the orthorhombic crystal system with the $P2_12_12_1$ and *Pbca* space symmetry, respectively (Table S1). The molecules of **2–4** are packed in the solid state via weak C − H···Cl, C − H···O and C − H···π intermolecular interactions. Complexes **2–4** feature mononuclear distorted square planar $PtClNP_2$ coordination polyhedra with a *cis* configuration for **2** and a *trans* configuration for **3** and **4** (Fig. 3). The sac ligand coordinates to Pt(II) through the negatively charged N atom.

The N–Pt–P angles in **3** and **4** are > 90° due to the steric hindrance between the phosphine and sac ligands (Table 1). The Pt − P bond distances (ca. 2.248 Å) in **2** are significantly shorter than those (ca. 2.315 Å) in **3** and **4**. These variations mainly depend on a combination of both electronic and steric properties of the tertiary phosphines bearing different R groups. The Me and Et substituents notably affect the electron-donating ability of the phosphine ligands [37,46]. More importantly, steric effects associated with the phosphine ligands have a greater impact on M − P bonds and can quantitatively be described using the Tolman's cone angle concept [37]. Previous structural data confirm that shorter M − P distances correspond to smaller cone angles of the PR_3 ligands [47]. The cone angles of 122, 140 and 136° reported for $PPhMe_2$, PPh_2Et and $PPhEt_2$, [37,48] respectively, correlate well with the Pt − P bond distances of the present complexes. In addition, the larger cone angles play an important role in the stereochemistry of the metal complexes and explain the *trans* configuration of the PPh_2Et and $PPhEt_2$ ligands in **3** and **4**.

The Pt − Cl bond distances in **2–4** are in close agreement with those reported in *cis*-$[PtCl(sac)(PPh_3)_2]$ [20], *cis*-$[PtCl(sac)(PPh_2Cy)_2]$ [22] and *trans*-$[PtCl(sac)(PPhCy_2)_2]$ [22]. Moreover, the Pt − Cl bond distance (ca. 2.34 Å) in **2** is considerably larger than those (ca. 2.30 Å) in **3** and **4**. The nature of the *trans* ligand obviously changes the Pt − Cl bond distances [49,50]. In **2**, the chlorido ligand is *trans* to $PPhMe_2$, whereas it is *trans* to sac in **3** and **4**. The greater *trans* influence of $PPhMe_2$ results in elongation of the Pt − Cl bonds in **2** and the weaker *trans* effect of sac gives the shorter Pt − Cl bonds in **3** and **4**. The Pt − N bond distances in **2–4** are in the range of recently reported Pt complexes of sac with mono and disphosphines [20–24]. On the other hand, the

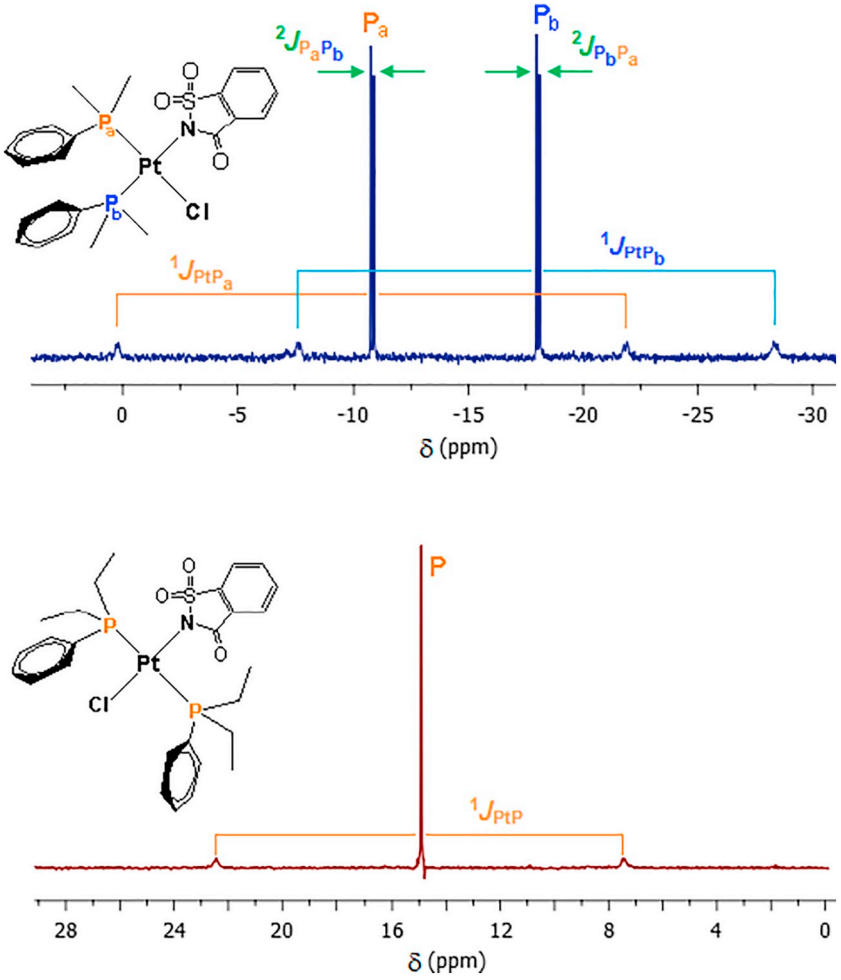

Fig. 1. $^{31}P\{^{1}H\}$ NMR spectra of *cis*-[PtCl(sac)($PPhMe_2$)$_2$] (**2**) and *trans*-[PtCl(sac)($PPhEt_2$)$_2$] (**4**) in DMSO-d_6 at rt.

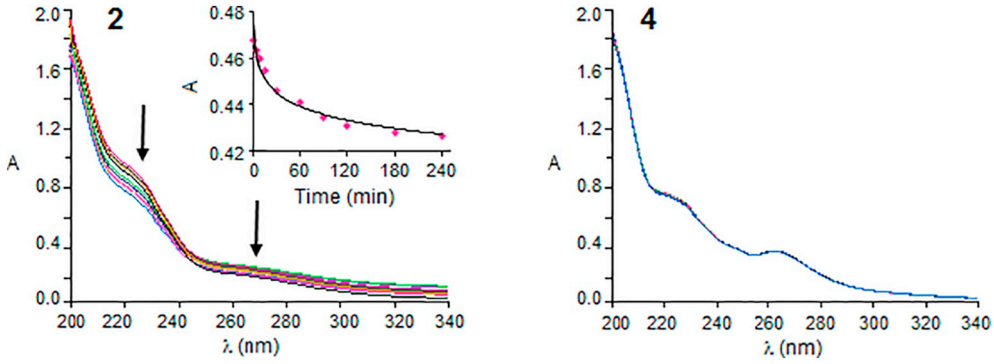

Fig. 2. Hydrolysis of *cis*- (**2**) and *trans*-configured complexes (**4**) in MeOH/H_2O (1/1, v/v) at 298 K recorded by a UV–vis spectrometer over a period of 4 h.

Pt − N bond distances (ca. 2.03 Å) in **3** and **4** are notably shorter than that (ca. 2.09 Å) in **2**, reflecting the higher *trans* effect of $PPhMe_2$ compared to that of the Cl^- ligand. In agreement with the ^{31}P NMR data, the *trans* effects of the ligands can be given in the order: $PPh_2R \approx PPhR_2 > > Cl^- > sac$.

3.4. DNA binding

Since cisplatin targets the nuclear DNA, the DNA binding capability of **1–4** was studied using different methods. As shown in Fig. S7, the incremental addition of the complexes in the solutions of fish sperm (FS) DNA results in hyperchromism in the absorbance of DNA at ca. 260 nm. The intrinsic binding constants (K_b) are estimated as 4.10 (± 0.11) × 10^4, 5.82 (± 0.04) × 10^4, 1.90 (± 0.08) × 10^3 and 5.29 (± 0.03) × 10^3 M^{-1} for **1–4**, respectively and indicate remarkably high binding affinity of the *cis*-configured complexes (**1** and **2**) towards DNA. Ethidium bromide (EB) is known to intercalate between the base pairs of DNA and the EB displacement experiments were performed to elucidate the mode of binding of the complexes to DNA. **1** and **2** exhibit greater emission quenching of the EB-DNA solutions, and also display a 4 nm red-shift (Fig. S8). The quenching constants (K_{SV}) are in the range of 1.13–3.13 × 10^4 M^{-1}, being less than those of classical intercalators (ca. 10^7 M^{-1}) and the phosphine complexes of Pt(II) (ca. 10^5 M^{-1}) [51], thus suggesting that these complexes most likely interact with FS-

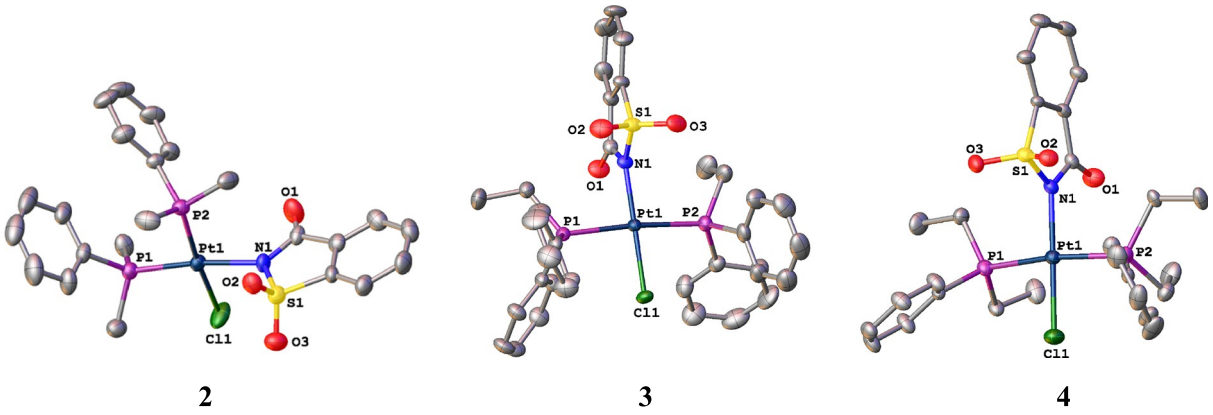

Fig. 3. Molecular structures of **2**–**4**.

Table 1
Selected bond lengths (Å) and angles (°) for **2**–**4**.

	2	3	4
Pt1 − Cl1	2.3383(19)	2.3021(14)	2.3028(16)
Pt1 − N1	2.087(5)	2.031(4)	2.029(4)
Pt1 − P1	2.2486(16)	2.3151(16)	2.3120(16)
Pt1 − P2	2.2470(17)	2.3229(17)	2.3044(16)
N1 − Pt1 − Cl1	87.12(16)	179.88(17)	177.86(13)
N1 − Pt1 − P1	172.59(16)	91.99(17)	93.38(13)
N1 − Pt1 − P2	90.60(16)	92.69(17)	92.23(13)
P1 − Pt1 − Cl1	85.74(7)	88.01(7)	87.40(6)
P2 − Pt1 − Cl1	174.17(8)	87.30(7)	87.24(6)
P1 − Pt1 − P2	96.70(6)	174.16(7)	171.01(6)

DNA via partial intercalation or groove binding. In addition, the binding constants (K_F) of **1** and **2** are ten-fold higher than those of **3** and **4** (Table S2). On the other hand, the viscosity of DNA is sensitive to the binding nature of molecules [52]. The viscosity of DNA was slightly increased in the presence of the complexes, similar to that of the groove binder (Hoechst 33258) (Fig. S9), thus proving that all the complexes bind to the grooves of DNA.

The nuclease activity of the complexes towards pBR322 plasmid DNA is monitored by the gel electrophoresis. As shown in Fig. 4a, the *cis*-configured complexes (**1** and **2**) reveal a dose-dependent cleavage activity, converting the supercoiled form (I) to the open circular form (II), whereas the *trans*-configured complexes (**3** and **4**) do not show any nuclease activity and even these complexes do not alter the electrophoretic mobility of DNA. However, **3** and **4** effectively cleave the plasmid DNA only in the presence of hydrogen peroxide. The binding modes of **1**–**4** were also clarified by gel electrophoresis. DAPI (4-,6-diamidino-2- phenylindole) and MG (methyl green) act as minor and major groove DNA binders, respectively. As shown in Fig. 4b, the *cis*- and *trans*-configured complexes display different DNA binding preferences. The DNA cleavage activity of **1** and **2** is inhibited by DAPI, whereas the nuclease activity of **3** and **4** in the presence of H_2O_2 is inhibited by MG. These observations demonstrate that the *cis*-configured complexes (**1** and **2**) act as a DNA minor groove binder, while the *trans*-configured complexes (**3** and **4**) interact with the major groove of DNA.

Molecular docking studies were performed to confirm the DNA binding modes. The energetically favourable docked poses obtained from the molecular docking of **2** and **4** with 1BNA show that the *cis*-configured complex (**2**) fits well into the G/C rich region the minor groove DNA, whereas the *trans*-configured complex (**4**) interacts with the A/T bases in the major groove of DNA (Fig. 5). Both complexes form strong N − H···O hydrogen bonds between the NH_2 group of G or A and the sulfonyl O atoms of sac. The free binding energy values of the docked structures are calculated as −30.12 kJ mol^{-1} for **2** and −24.69 kJ mol^{-1} for **4**, in agreement with the experimental values of −29.80 kJ mol^{-1} for **2** and −23.79 kJ mol^{-1} for **4** (Table S2). The binding modes and energy values obtained from molecular docking are consistent with the experiments, indicating much greater DNA binding affinity of the *cis*-configured complexes over their *trans*-congeners.

3.5. Lipophilicity and cellular uptake

Two factors usually contributing to the metal-based drug cytotoxicity are both lipophilicity and cellular uptake. The lipophilicity of a

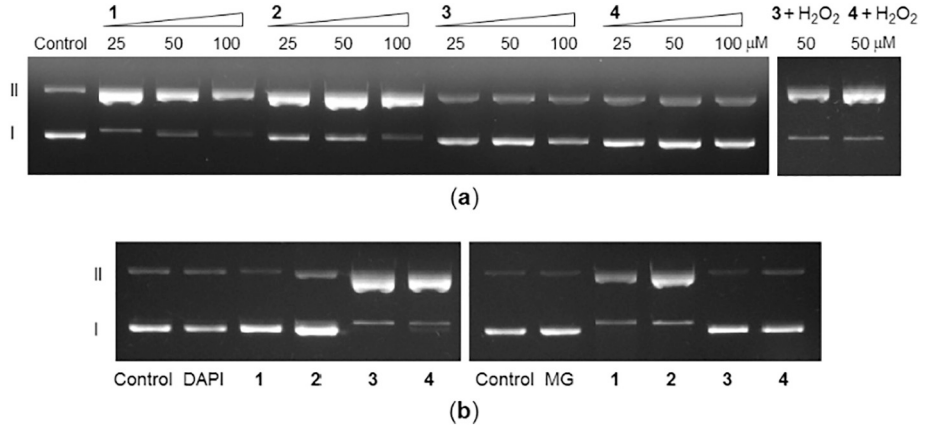

Fig. 4. (**a**) Nuclease activity of **1**–**4** on pBR322 plasmid DNA (25 μM bp). [H_2O_2] = 100 μM. (**b**) The DNA cleavage activity of the complexes in the presence of groove binders DAPI and MG.

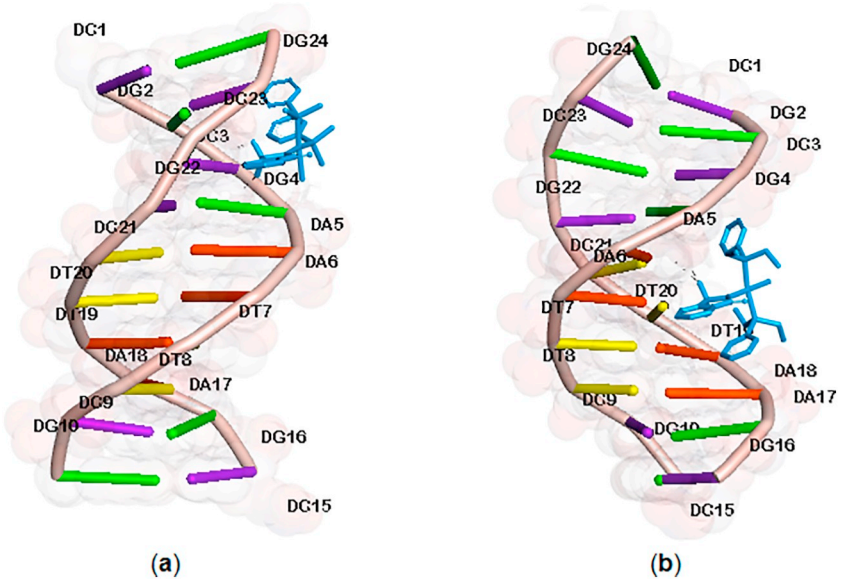

Fig. 5. Molecular docked models of **2** (**a**) and **4** (**b**) with DNA (PDB ID: 1BNA).

Table 2
Lipophilicity[a], Pt uptake[b] and anticancer activity[c] of **1**, **2** and cisplatin.

		1	2	Cisplatin
log *P*		1.25 ± 0.02	1.34 ± 0.02	−2.28 ± 0.07
Pt uptake		99.4 ± 5.2	115.2 ± 6.1	25.9 ± 1.4
A549	GI_{50}	16.42 ± 0.85	24.56 ± 4.34	14.38 ± 0.47
	TGI	29.13 ± 1.43	> 40	22.63 ± 0.38
	LC_{50}	> 40	> 40	37.77 ± 0.65
MCF-7	GI_{50}	7.38 ± 0.64	5.38 ± 0.03	10.88 ± 0.18
	TGI	13.40 ± 0.66	22.06 ± 0.57	15.19 ± 0.10
	LC_{50}	18.93 ± 0.64	38.64 ± 0.68	19.50 ± 0.01
HCT116	GI_{50}	12.19 ± 0.26	12.72 ± 1.55	9.03 ± 1.46
	TGI	17.12 ± 0.23	24.39 ± 2.53	21.24 ± 1.71
	LC_{50}	28.18 ± 0.49	> 40	34.28 ± 1.10
BEAS-2B	GI_{50}	8.52 ± 0.63	21.46 ± 0.76	3.85 ± 0.03
	TGI	14.06 ± 0.81	31.06 ± 0.59	6.18 ± 0.17
	LC_{50}	26.95 ± 2.56	> 40	10.83 ± 1.24

[a] Measured using the shake-flask method.
[b] pmol platinum complex per million MCF-7 cells after a 4 h exposure time at 25 μM concentration.
[c] In vitro activity in μM determined by the ATP assay after 48 h treatment with the complexes. GI_{50} = dose of 50% growth inhibition, TGI = dose of total growth inhibition and LC_{50} = dose of 50% cell death.

compound is a combination of its hydrophilic and hydrophobic characters. The octanol/water partition coefficients, referred to as log *P* in Table 2 were determined to assess the lipophilicity of **1**–**4** and cisplatin. The log *P* values of **1**–**4** are 1.25 ± 0.02, 1.34 ± 0.02, 1.38 ± 0.02 and 1.51 ± 0.02, respectively. Comparing to cisplatin (log *P* = −2.28), the complexes are sufficiently lipophilic to satisfy the general requirement of drugs [53]. The number of Me, Et and Ph groups in the tertiary phosphines has an apparent effect on the lipophilicity of the complexes, while the sac ligand presents both polar and nonpolar groups. Therefore, the lipophilic character of the complexes is mainly stimulated by the hydrophobic nature of PPh_2Me, $PPhMe_2$, PPh_2Et and $PPhEt_2$.

The cellular levels of **1**–**4** were determined to examine accumulation of the complexes after a 4 h exposure of 25 μM of each complex to MCF-7 cells. The total complex uptake by MCF-7 cells is estimated as 99.4 ± 5.2, 115.2 ± 6.1, 112.3 ± 6.8, 117.8 ± 5.5 pmol complex/10^6 cells for **1**–**4**, respectively. The uptake of the new platinum complexes was approximately 5-fold greater than that of cisplatin (Table 2).

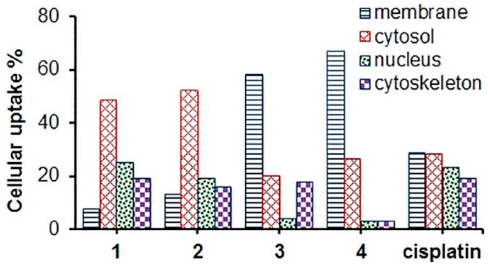

Fig. 6. Subcellular distribution of **1**–**4** and cisplatin in MCF-7 cells.

The higher uptake of the present complexes correlates well their much higher lipophilicity. The distribution of **1**–**4** in the subcellular fractions such as cytosol, membrane, cytoskeleton and nucleus is shown in Fig. 6. Complexes **1** and **2** present similar profiles, i.e., a high amount in the cytosol and low retention in the membrane, whereas **3** and **4** tend to accumulate in the membrane and cytosol fractions. It should be noted that a significant portion of **1**, **2** and cisplatin is found in the nucleus, giving access to the nuclear DNA.

3.6. Anticancer activity

In vitro anticancer activity of complexes **1**–**4** was evaluated by the SRB assay at a single dose (20 μM) on a panel of three most common human cancer cell lines of lung (A549), breast (MCF-7), colon (HCT116) and one normal human bronchial epithelial cell line (BEAS-2B). At the single dose assay, the *cis*-configured complexes (**1** and **2**) displayed remarkable activity against all the cell lines, whereas only HCT116 cells showed relatively weak sensitivity towards the *trans*-configured complexes (**3** and **4**) (Fig. S10).

In order to investigate the dose response parameters of the National Cancer Institute (NCI), the most active complexes (**1** and **2**) were further tested by the ATP assay, along with the reference platinum complex cisplatin, for antiproliferative, cytostatic and cytotoxic activities. Each complex was tested at seven different doses between 0.63 and 40 μM. The results are expressed as GI_{50} (50% growth inhibition, the growth inhibitory effect), TGI (100% growth inhibition, the cytostatic effect), and LC_{50} values (the dose killing 50% of the cells, the cytotoxic effect) (Table 2 and Fig. 7). A549 is the least sensitive cell line, although **1** is more active than **2** in this cell line. Both complexes show better cytotoxic activity against MCF-7 cells regarding to their relatively lower

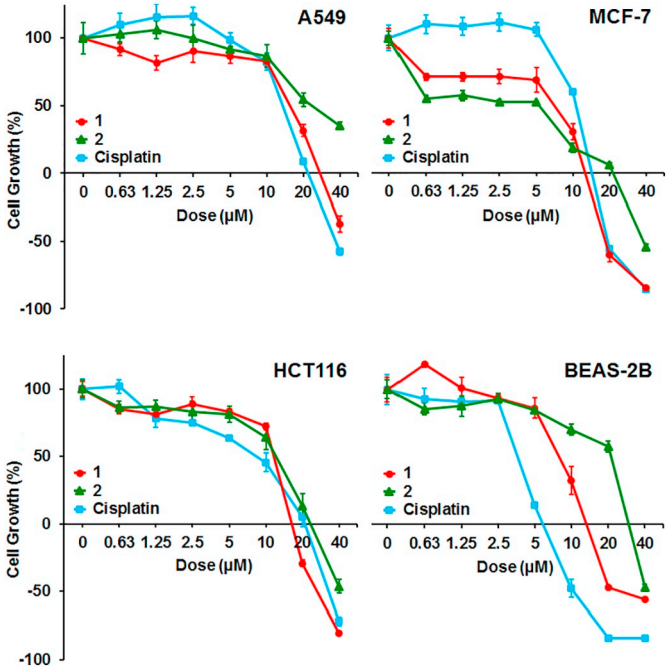

Fig. 7. Dose response curves after 48 h treatment of the cells with **1**, **2** and cisplatin. +50% = growth inhibition (GI_{50}), 0% = cytostatic effect (TGI) and −50% = cytotoxic effect (LC_{50}).

GI_{50}, TGI and LC_{50} values compared to other cancer cells (HCT116 and A549). **1** has somewhat higher cytotoxic and cytostatic effects than cisplatin in MCF-7 and HCT116 cells, but these effects are less pronounced for **2**. In addition, MCF-7 cells are most sensitive to the antiproliferative effects of these complexes so that **1** and **2** seem to cause stronger antiproliferation in the range of 0.63–10 μM in comparison with cisplatin.

Pervious work has shown that the stereochemistry at the Pt(II) centre plays a great role in affecting the anticancer activity of platinum complexes [54,55]. The results of the present study indicate that the *cis*-configured complexes (**1** and **2**) display high anticancer potency over their *trans* counterparts (**3** and **4**). Moreover, a structurally similar platinum(II) complex, *trans*-[PtCl(sac)$(PCy_3)_2$], did not show any anticancer activity [22]. There are not significant differences between the log *P* values of **1**–**4**. Even, **3** and **4** have slightly higher lipophilicity. Therefore, it is not reasonable to attribute the higher anticancer activity of **1** and **2** to the hydrophobic effects. The total cellular uptake of the complexes by MCF-7 cells is in the same order and it is assumed that the complexes may readily enter the cells. However, the distribution of the complexes in the subcellular fractions indicates a relatively higher portion of **1** and **2** in the nucleus, which may be responsible for their higher cytotoxicity.

Another possible explanation is that the toxicity of the complexes may be determined by their reactivity towards DNA. Especially the *cis*-configured complexes show much greater binding affinity against DNA as deduced from DNA binding and nuclease activity studies. Since the aqua complexes of Pt(II) react readily with DNA nucleobases, the hydrolysis of **1** and **2** favours the reaction of these complexes with DNA. As a result, **1** and **2** can be considered as DNA targeting agents and the mechanistic studies explained below are further confirmed DNA targeting properties of these complexes within living cells.

3.7. Anticancer mechanism

In vitro studies showed that the *cis*-configured complexes (**1** and **2**) show promising activity especially against MCF-7 and HCT116 cells. Flow cytometry analyses of apoptosis, cell cycle progression, generation of reactive oxygen species (ROS), mitochondrial membrane depolarization and DNA damage were evaluated to understand the impact of both complexes on cell growth. In addition, changes in the nuclear morphology were studied by the Hoechst 33342 staining. For this purpose, MCF-7 cells were selected and treated with the IC_{90} doses of **1** (27.2 μM), **2** (44.5 μM) and cisplatin (28.0 μM) for different time intervals.

3.7.1. Apoptosis induction

3.7.1.1. Nuclear staining. Apoptosis can be identified by the occurrence of morphological alterations in cells. Such changes in the morphology of nuclei of MCF-7 cells treated with **1**, **2** and cisplatin were followed by fluorescence microscope using the DNA binding dye Hoechst 33342. As shown in Fig. 8, the untreated cells display uniform appearance. After treatment with the complexes, the number of cells significantly decreased and the cells became smaller in size due to the cell shrinkage in a time-dependent manner. In addition, pyknotic nuclei are apparent, indicating the condensation of chromatin. Moreover, fragmented nuclei can also be seen in the treated cells at 12 and 24 h. These morphological alterations clearly suggest induction of apoptosis in MCF-7 cells by **1** and **2**.

3.7.1.2. Annexin V staining. Annexin V staining assay was performed to further analyse the nature of cell death. MCF-7 cells showed Annexin-V positivity, shifting to the late apoptotic stage after incubation with **1**, **2** and cisplatin for 24 and 48 h (Figs. 9a and S11). In the presence of both complexes, > 77% cells are detected to be apoptotic at 24 h, and a total of 94% and 88% of cells undergoes apoptosis at 48 h, in the case of **1** and **2**, respectively. Further, ca. 17 and 10% of cells treated with **2** and cisplatin, respectively, were found in the early apoptotic stage at 24 h. It should be emphasized that **1** showed notably enhanced ability to induce apoptosis of MCF-7 cells, being consistent with its higher anticancer activity compared to **2** and cisplatin. These findings clearly confirmed

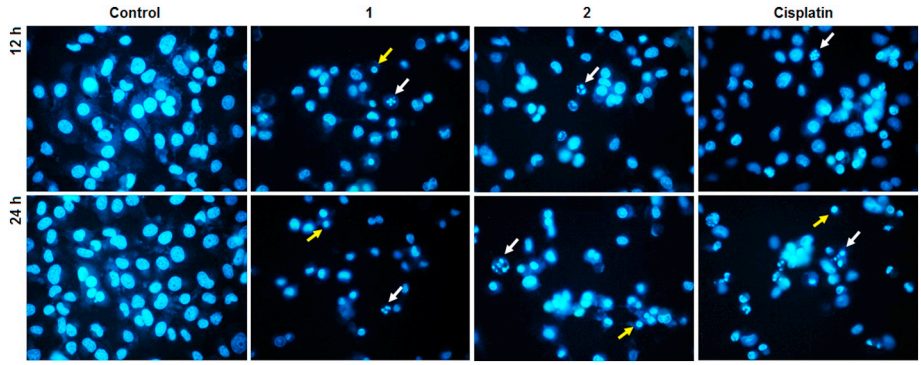

Fig. 8. Hoechst 33342 staining of MCF-7 cells treated with **1**, **2** and cisplatin for 12 and 24 h, showing the changes in nuclear morphology. White and yellow arrows show fragmented and pyknotic nuclei, respectively. Magnification: 40×.

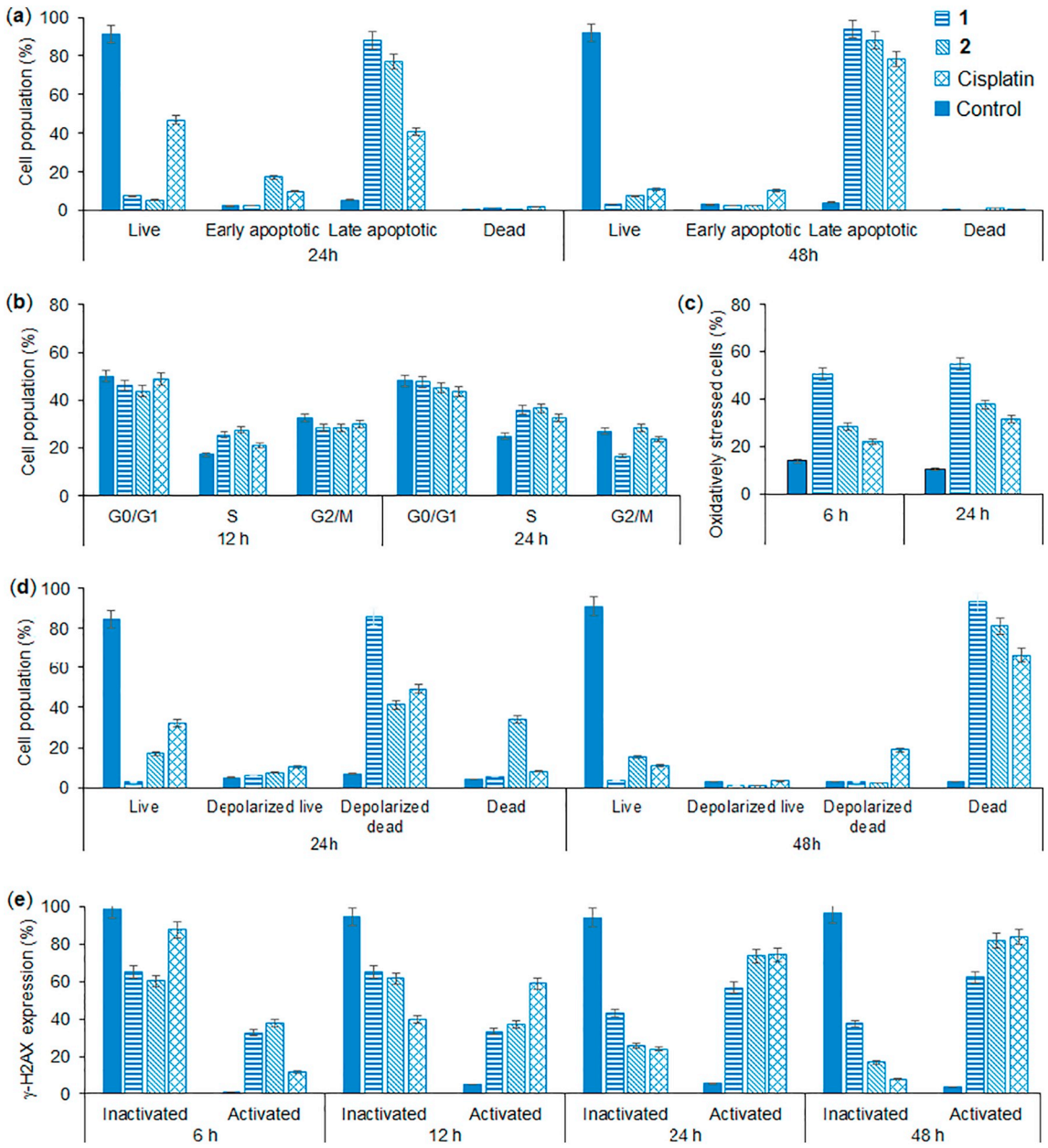

Fig. 9. Flow cytometry analysis of MCF-7 cells exposed to IC_{90} doses of **1** (27.2 μM), **2** (44.5 μM) and cisplatin (28.0 μM) at different time intervals. (**a**) Annexin V activity, (**b**) Cell cycle progression, (**c**) ROS production, (**d**) depolarization of mitochondrial membrane and (**e**) DNA double-strand breaks.

that these complexes can induce cell death through the apoptotic pathway.

3.7.2. Cell cycle progression

The growth of cells is obviously influenced due to the toxicity of anticancer drugs. Since **1** and **2** displayed similar cytotoxicity, their effect on the cell cycle progression was investigated. The treatment of MCF-7 cells with **1** and **2** effectively arrested the cells in the S phase of the cell cycle. The population of MCF-7 cells in both G0/G1 and G2/M phases was reduced, while cells in the S phase increased by approximately 10% at 12 and 24 h compared to that of control cells (Figs. 9b and S12). At 24 h, over 36% of the cell population accumulated in S-phase in response to the activity of the complexes. The percentage of the cells in the S phase was notably higher in the case of the complexes, compared that for cisplatin. The S phase is related to the DNA synthesis stage in the cell progression and cisplatin is known to block the cell cycle at the S phase in various human cancer cells [56]. These results point out that **1** and **2** meditate the S phase arrest of the treated MCF-7 cells and thus, block DNA replication, leading to cell death.

3.7.3. Oxidative stress

Several studies demonstrated that the anticancer effects of platinum-based chemotherapeutic drugs are closely related to increased ROS generation [57–59]. The oxidative stress induced by **1**, **2** and cisplatin in MCF-7 cells was measured to investigate whether the cytotoxic effect of these complexes is related with ROS production. As shown in Figs. 9c and S13, the ROS levels increased significantly with the treatment of the cells with the complexes for 6 and 24 h. The amount of oxidatively stressed cells was ca. 12% in the control. In the case of **1**, the percentage of cells with oxidative stress was over 50% at both 6 and 24 h, whereas two- and three-fold increases in the amount of stressed cells were recorded in **2** and cisplatin treated cells. These results strongly suggest that both complexes are able to induce oxidative stress due to excessive generation of intracellular ROS. Complex **1** gives

rise to high ROS levels in cells especially at early times. However, **2** and cisplatin induce comparatively low ROS levels at 6 h, and longer exposure of cells with these complexes results in increased ROS production. Since the excessive amounts of ROS can cause destructive effects, in particular, triggering the apoptotic pathway including alteration of the mitochondrial membrane potential and damage to genomic DNA, it may be responsible for the cell toxicity of these complexes.

3.7.4. Depolarization of mitochondrial membrane

The mitochondria are considered as an essential part of the intrinsic apoptotic pathway. Loss of mitochondrial membrane integrity induces the release of apoptotic effectors that initiate the death signalling cascade [60]. The alterations in the permeability of mitochondrial membrane can be assessed by measuring changes in depolarization of the mitochondrial membrane. The results presented in Figs. 9d and S14 show that 92% of MCF-7 cells treated with **1** for 24 h have depolarized mitochondrial membranes. In the case of **2** and cisplatin, the percentage of cells with depolarized mitochondria is 49 and 60% at 24 h, respectively. At the meanwhile, 34 and 8% of cells are dead in the case of **2** and cisplatin, respectively. Most of the cells exposed to **1** and **2** for 48 h are found in the dead stage, whereas cisplatin causes 22 and 67% of depolarized and dead cells, respectively. The present results indicate that the mitochondrial membrane in MCF-7 cells are highly depolarized by the presence of both complexes at 24 h. The effect of **1** is much more prominent, correlating well with its high efficiency in ROS formation. As a result, it can be concluded that mitochondrial dysfunction is involved in death of MCF-7 cells induced by the complexes.

3.7.5. DNA damage

DNA double-strand breaks (DSBs) in cells can occur as a result of metabolic reactions such as ROS or exposure to chemotherapeutics [61]. The clinically-used anticancer platinum drugs are known to bind covalently to DNA strands and induce DNA damage [62,63]. The results of the present work show that **1** and **2** target DNA as deduced from DNA binding and nuclease activity studies, and increase the generation of ROS. Therefore, the amount of DSBs in MCF-7 cells treated with **1**, **2** and cisplatin for 6, 12, 24 and 48 h was detected by H2AX assay. H2AX is a member of the H2A protein family and increasingly used as a biomarker of DSBs, owing to the phosphorylation of this variant at the Ser139 residue, called γ-H2AX, in response to DNA damage [64–66]. As shown in Figs. 9e and S15, both complexes induce significant increase in the formation of DSBs in a time-dependent manner in MCF-7 cells, as stated 'activated'. At 6 h, 3-fold higher γ-H2AX expression is recorded for the complexes compared to cisplatin, indicating higher DNA damage induced by the complexes at earlier times of treatment. However, cisplatin produces increased γ-H2AX expression at 12 h and the γ-H2AX levels at 24 and 48 h are similar to those induced by **2**. On the other hand, in comparison with **2** and cisplatin, the γ-H2AX percentage is considerably smaller in the case of **1** at 24 and 48 h. These results show that the complexes cause DSBs in nuclear DNA in MCF-7 cells that results in high increases in γ-H2AX. The DNA damage may arise from strong interactions of the complexes with DNA or elevated levels of ROS induced by the complexes.

4. Conclusions

A series of chlorido platinum(II) saccharinate complexes containing PPh_2Me, $PPhMe_2$, PPh_2Et and $PPhEt_2$ were prepared and fully characterized by spectroscopic methods. The structures of three complexes were determined by X-ray crystallography. The PPh_2Me and $PPhMe_2$ ligands coordinate Pt(II) in a *cis* fashion, while the coordination of PPh_2Et and $PPhEt_2$ ligands results in the *trans* geometry. Various physico- and biochemical techniques demonstrate that the *cis*-configured complexes (**1** and **2**) show much higher affinity towards the minor grooves of DNA, while the *trans*-configured complexes (**3** and **4**) moderately bind to the major grooves of DNA.

The *cis*-configured complexes (**1** and **2**) display high anticancer activity towards MCF-7 and HCT116 cancer cells, whereas the *trans*-configured complexes (**3** and **4**) are not biological active. Although all the complexes exhibit higher lipophilicity and higher cellular uptake compared to cisplatin. It was shown that the *cis*-configured complexes (**1** and **2**) undergo the hydrolysis forming aqua species in aqueous solution, whereas the hydrolysis of the *trans*-configured complexes (**3** and **4**) does not occur. Therefore, enhanced anticancer activity of **1** and **2** can be explained by their higher affinity towards the nuclear DNA due to the formation of their aqua species in cell culture.

1 and **2** are selected for further biological investigation on their mechanism of action in MCF-7 cells. Both complexes arrest the cell cycle progression in the DNA synthesis phase (S) and induce apoptotic cell death. In addition, these complexes significantly increase the generation of ROS, which consequently alter depolarization of the mitochondrial membrane and damage the nuclear DNA. In conclusion, the *cis*-configured complexes can be considered as mitochondrial and DNA-targeting anticancer agents.

Abbreviations

ATCC	American Type Culture Collection
ATP	adenosine triphosphate
COD	1,5-cyclooctadiene
DAPI	4-,6-diamidino-2-phenylindole
DMF	*N*,*N*-dimethyl formamide
DMSO	dimethyl sulfoxide
DSBs	DNA double-strand breaks
EB	ethidium bromide
FS-DNA	fish sperm DNA
MG	methyl green
ROS	reactive oxygen species
RPMI	Roswell Park Memorial Institute medium
SRB	Sulforhodamine B
TBE	Tris-borate-EDTA

Acknowledgements

The financial support for the research project (215Z230) from TUBITAK is gratefully acknowledged. The authors thank Prof. Dr. Ismail Ozdemir (Inonu University) for collecting NMR spectroscopic data.

Appendix A. Supplementary data

Supplementary data to this article can be found online at https://doi.org/10.1016/j.jinorgbio.2019.03.008.

References

[1] S.M. Aris, N.P. Farrell, Eur. J. Inorg. Chem. 10 (2009) 1293–1302.
[2] R. Oun, Y.E. Moussa, N.J. Wheate, Dalton Trans. 47 (2018) 6645–6653.
[3] E. Guney, V.T. Yilmaz, F. Ari, O. Buyukgungor, E. Ulukaya, Polyhedron 30 (2011) 114–122.
[4] F. Ari, N. Aztopal, C. Icsel, V.T. Yilmaz, E. Guney, O. Buyukgungor, E. Ulukaya, Bioorg. Med. Chem. 21 (2013) 6427–6434.
[5] E. Ulukaya, F. Ari, K. Dimas, M. Sarimahmut, E. Guney, N. Sakellaridis, V.T. Yilmaz, J. Cancer Res. Clin. Oncol. 137 (2011) 1425–1434.
[6] E. Ulukaya, F. Ari, K. Dimas, E.I. Ikitimur, E. Guney, V.T. Yilmaz, Eur. J. Med. Chem. 46 (2011) 4957–4963.
[7] Z. Adiguzel, A.T. Baykal, O. Kacar, V.T. Yilmaz, E. Ulukaya, C. Acilan, J. Proteome Res. 13 (2014) 5240 − 5249.
[8] E.I. Ikitimur-Armutak, K. Sonmez, K. Akgun-Dar, G. Sennazli, A. Kapucu, F. Yigit, V.T. Yilmaz, E. Ulukaya, Anticancer Res. 35 (2015) 1491 − 1497.
[9] E.I. Ikitimur-Armutak, E. Ulukaya, E. Gurel-Gurevin, I. Yaylim, B. Isbilen-Basok, G. Sennazli, G. Yuzbasioglu-Ozturk, K. Sonmez, F. Celik, O. Kucukhuseyin, G. Korkmaz, V.T. Yilmaz, S.U. Zeybek, In Vivo 30 (2016) 457 − 464.
[10] Y. Cetin, Z. Adiguzel, H.U. Polat, T. Akkoc, A. Tas, B. Cevatemre, G. Celik, B. Carikci, V.T. Yilmaz, E. Ulukaya, C. Acilan, Anti-Cancer Drugs 28 (2017) 898–910.

[11] M. Cavicchioli, A.C. Massabni, E.E. Castellano, L.P.B. Sabeh, C.M. Costa-Neto, Inorg. Chim. Acta 360 (2007) 3055–3060.
[12] S.A. Al-Jibori, G.H. Al-Jibori, L.J. Al-Hayaly, C. Wagner, H. Schmidt, S. Timur, F.B. Barlas, E. Subasi, S. Ghosh, G. Hogarth, J. Inorg. Biochem. 141 (2014) 55–57.
[13] K. Karami, M. Alinaghi, Z. Amirghofran, J. Lipkowskic, A.A. Momtazi-borojeni, New J. Chem. 42 (2018) 574–586.
[14] P. Bergamini, V. Bertolasi, L. Marvelli, A. Canella, N. Mantovani, S. Manas, A. Romerosa, Inorg. Chem. 46 (2007) 4267–4276.
[15] N. Cutillas, A. Martinez, G.S. Yellol, V. Rodrigez, A. Zamora, M. Pedreno, A. Donaire, C. Janiak, J. Ruiz, Inorg. Chem. 52 (2013) 13529–13535.
[16] J. Albert, J. Granell, R. Qadir, J. Quirante, C. Calvis, R. Messeguer, J. Badia, L. Boldama, M. Font-Bardia, T. Calvet, Organomet 33 (2014) 7284–7292.
[17] M.D. Zivkovic, J. Kljun, T. Ilic-Tomic, A. Pavic, A. Veselinovic, D.D. Monojlovic, J. Nikodinovic-Runic, I. Turel, Inorg. Chem. Front. 5 (2018) 39–53.
[18] S.J. Berners-Price, P.J. Sadler, Struct. Bond. 70 (1988) 27–102.
[19] J.C. Shi, L.J. Cheng, X.Y. Huang, D.X. Wu, B.S. Kang, J. Organomet. Chem. 535 (1997) 17–23.
[20] W. Henderson, B.K. Nicholson, L.J. McCaffrey, Inorg. Chim. Acta 285 (1999) 145–148.
[21] S.A. Al-Jibori, A.I.A. Al-Nassiry, G. Hogarth, L. Salassa, Inorg. Chim. Acta 398 (2013) 46–53.
[22] V.T. Yilmaz, C. Icsel, O.R. Turgut, M. Aygun, M. Erkisa, M.H. Turkdemir, E. Ulukaya, Eur. J. Med. Chem. 155 (2018) 609–622.
[23] C. Icsel, V.T. Yilmaz, M. Aygun, B. Cevatemre, P. Alper, E. Ulukaya, Dalton Trans. 47 (2018) 11397–11410.
[24] V.T. Yilmaz, C. Icsel, M. Aygun, M. Erkisa, E. Ulukaya, Eur. J. Med. Chem. 158 (2018) 534–547.
[25] G.M. Sheldrick, Acta Cryst. A 71 (2015) 3–8.
[26] G.M. Sheldrick, Acta Cryst. C 71 (2015) 3–8.
[27] O.V. Dolomanov, L.J. Bourhis, R.J. Gildea, J.A.K. Howard, H. Puschmann, J. Appl. Crystallogr. 42 (2009) 339–341.
[28] OECD Method, Partition Coefficient (N-Octanol/Water): Shake Flask Method, (1995).
[29] J. Messersehmidt, F. Alt, G. Tolg, J. Angerer, K.H. Schaller, Fresenius J. Anal. Chem. 343 (1992) 391–394.
[30] H.A. Benesi, J.H.A. Hildebrand, J. Am. Chem. Soc. 71 (1949) 2703–2707.
[31] O. Stern, M. Volmer, Z. Phys. 20 (1919) 183–188.
[32] M. Lee, A.L. Rhodes, M.D. Wyatt, S. Forrow, J.A. Hartley, Biochem 32 (1993) 4237–4245.
[33] J. Min, X.M. Meng-Xia, Z. Dong, L. Yuan, L. Xiao-Yu, C. Xing, J. Mol. Struct. 692 (2004) 71–80.
[34] O. Trott, A.J. Olson, J. Comput. Chem. 31 (2010) 455–461.
[35] J. Kritzenberger, H. Yersin, K.J. Range, M. Zabel, Z. Naturforsch. 49b (1994) 297–300.
[36] W.A. Henderson Jr., C.A. Streuli, J. Am. Chem. Soc. 82 (1960) 5791–5794.
[37] C.A. Tolman, Chem. Rev. 77 (1977) 313–348.
[38] B.C. Ankianiec, V. Christou, D.T. Hardy, S.K. Thomson, G.B. Young, J. Am. Chem. Soc. 116 (1994) 9963–9978.
[39] L. Bemi, H.C. Clark, J.A. Davies, C.A. Fyfe, R.E. Wasylishen, J. Am. Chem. Soc. 104 (1982) 438–445.
[40] L. Rigamonti, A. Forni, M. Manassero, C. Manassero, A. Pasini, Inorg. Chem. 49 (2010) 123–135.
[41] Z. Kokan, B. Peric, G. Kovacevic, A. Brozovic, N. Metzler-Nolte, S.I. Kirin, Eur. J. Inorg. Chem. 2017 (2017) 3928–3937.
[42] S.J. Berners-Price, L. Ronconi, P.J. Sadler, Prog. Nucl. Magn. Reson. Spectrosc. 49 (2006) 65–98.
[43] J.C. Dabrowiak, Metals in Medicine, Wiley, West Sussex, UK, 2009.
[44] G.Y. Park, J.J. Wilson, Y. Song, S.J. Lippard, Proc. Natl. Acad. Sci. U. S. A. 109 (2012) 11987–11992.
[45] T. Chatzisideri, S. Thysiadis, S. Katsamakas, P. Dalezis, I. Sigala, T. Lazarides, E. Nikolakaki, D. Trafalis, O.A. Gederaas, M. Lindgre, V. Sarli, Eur. J. Med. Chem. 141 (2017) 221–231.
[46] C.A. Tolman, J. Am. Chem. Soc. 92 (1970) 2953–2956.
[47] G.A. Ardizzoia, S. Brenna, Phys. Chem. Chem. Phys. 19 (2017) 5971–5978.
[48] J.A. Bilbrey, A.H. Kazez, J. Locklin, W.D. Allen, J. Comp. Chem. 34 (2013) 1189–1197.
[49] P. Kapoor, K. Lovqvist, A. Oskarsson, J. Mol. Struct. 470 (1998) 39–47.
[50] P.N. Kapoor, R. Kakkar, THEOCHEM J. Mol. Struct. 679 (2004) 149–156.
[51] M. Jamshidia, R. Yousefi, S.M. Nabavizadeh, M. Rashidi, M.G. Haghighi, A. Niazi, A.-A. Moosavi-Movahedid, Int. J. Biol. Macromol. 66 (2014) 86–96.
[52] D. Suh, J.B. Chaires, Bioorg. Med. Chem. 3 (1995) 723–728.
[53] P.D. Leeson, B. Springthorpe, Nat. Rev. Drug Discov. 6 (2007) 881–890.
[54] F.J. Ramos-Lima, A.G. Quiroga, B. Garcia-Serrelde, F. Blanco, A. Carnero, C. Navarro-Ranninger, J. Med. Chem. 50 (2007) 2194–2199.
[55] W. Zhou, M. Almeqdadi, M.E. Xifaras, I.A. Riddell, O.H. Yilmaz, S.J. Lippard, Chem. Commun. 54 (2018) 2788–2791.
[56] P. Wang, J. Cui, J. Wen, Y. Guo, L. Zhang, X. Chen, Oncol. Lett. 12 (2016) 4851605–4854612.
[57] A. Miyajima, J. Nakashima, K. Yoshioka, M. Tachibana, H. Tazaki, M. Murai, Br. J. Cancer 76 (1997) 206–210.
[58] N.I. Weijl, G.D. Hopman, A. Wipkink-Bakker, E.G.W.M. Lentjes, H.M. Berger, F.J. Cleton, S. Osanto, Ann. Oncol. 9 (1998) 1331–1337.
[59] T. Itoh, R. Terazawa, K. Kojima, K. Nakane, T. Deguchi, M. Ando, Y. Tsukamasa, M. Ito, Y. Nozawa, Free Radic. Res. 45 (2011) 1033–1039.
[60] C. Wang, R.J. Youle, Ann. Rev. Genet. 43 (2009) 95–118.
[61] A. Mehta, J.E. Haber, Cold Spring Harb. Perspect. Biol. 6 (2014) a016428.
[62] S. Dasari, P.B. Tchounwou, Eur. J. Pharmacol. 740 (2014) 364–378.
[63] V. Brabec, O. Hrabina, J. Kasparkova, Coord. Chem. Rev. 351 (2017) 2–31.
[64] D.R. Pilch, O.A. Sedelnikova, C. Redon, A. Celeste, A. Nussenzweig, W.M. Bonner, Biochem. Cell Biol. 81 (2003) 123–129.
[65] L.J. Kuo, L.-X. Yang, In Vivo 22 (2008) 305–309.
[66] V. Turinetto, C. Giachino, Nucleic Acids Res. 43 (2015) 2489–2498.